

# Linear and Nonlinear Reduced-Order Modeling for Hypersonic Panel Flutter

Joe Schoneman\* and Christopher Ostoich†  
*ATA Engineering, Inc.; Huntsville, Alabama 35806*

Lucas Jarman‡  
*Georgia Institute of Technology; Atlanta, GA 30332*

Christopher Van Damme§ and Matthew S. Allen\*\*  
*University of Wisconsin-Madison; Madison, Wisconsin 53706*

**A common paradigm for the analysis of unsteady hypersonic aeroelasticity is the use of an approximate unsteady aerodynamic theory together with a structural finite element model. Of the available approximate techniques, piston theory approximations are popular for modeling the high-supersonic/low-hypersonic regime of Mach 4 to 7. Introducing the piston theory approximation allows unsteady pressures to be written as a closed-form function of the local displacement and velocity everywhere on a structure’s surface. Once such an approximation is applied to the coupled aerostructural problem, the use of a nonlinear finite element code becomes the major performance bottleneck. Adapting a reduced-order model based on the structure’s normal modes allows efficient evaluation of the structural equations of motion, but the common linear modal approximation omits important geometric nonlinearity effects in the structure. Geometric nonlinearity leads to stiffening at high amplitudes which is necessary for correct prediction of postflutter panel behavior. Nonlinear reduced-order models provide a method to maintain the computational efficiency of the linear modal model while attaining much more accurate results. This paper examines in detail the effect of using various combinations of linear/nonlinear piston theory and structural models to ascertain the importance of nonlinearities in each physical domain. The results confirm that, for classical flutter analysis, neither nonlinear aerodynamics nor nonlinear structural models need be included in the model, as long as both domains are correctly linearized from an initial base state. For meaningful postflutter analysis, a nonlinear structural model must be included along with nonlinear piston theory. Finally, the existence of amplitude-dependent instabilities resulting from nonlinear aerodynamics is observed in an aerothermoelastic test case.**

## I. Introduction

Hypersonic aircraft present a challenging multidisciplinary design and optimization problem. Operating at high Mach numbers, these vehicles must withstand extreme aerothermal loads while carrying a minimal amount of structural mass. Coupled high-fidelity analysis tools—computational fluid dynamics (CFD) codes working in concert with nonlinear finite element programs—are essential for the robust design of hypersonic aircraft. However, the high computational cost of full-fidelity coupled tools renders them unwieldy for certain applications, particularly fatigue or flutter analysis, which require repeated evaluations of the fluid and structure at small timescales over relatively long time histories. Flutter evaluation at a single point along a flight trajectory may require thousands of function evaluations to numerically integrate the system; a single fatigue evaluation may require millions. To bring the cost of such procedures down to a reasonable level, reduced-fidelity/reduced-order methods are commonly employed.

---

\* Engineer; AIAA Member

† Project Engineer

‡ Graduate student; Department of Aerospace Engineering; AIAA Student Member

§ Graduate student; Department of Engineering Physics; AIAA Student Member

\*\* Associate professor, Department of Engineering Physics; AIAA Member

Piston theory is often used as an efficient and relatively accurate method to compute unsteady aerodynamic loads at hypersonic Mach numbers [1]. Eckert's reference enthalpy, commonly used in conjunction with piston theory, provides a semi-empirical method to determine transient heating rates based on the flow conditions and local pressure [2]. Finally, the structural problem can be reduced in size by projecting the structural equations of motion into a reduced set of degrees of freedom based on the normal modes of the structure. Numerous panel flutter studies have been performed by using a Galerkin procedure to analytically project a small set of modes (usually between two and six) onto the appropriate elastic structural model; see, for instance, references [3], [4], and [5]. This technique is theoretically well founded but it is limited in terms of the geometries and material nonlinearities that can be considered, since analytical mode functions are only known for simple structures such as square plates or infinite cylinders. In the context of modern finite element models (FEMs), a more common practice is to use either the linear mass and stiffness matrices or the linear normal modes of the structure, linearized about a particular equilibrium point with the flow, to form linear dynamic equations of motion for flutter analysis.

The use of a linear structural model computed from a FEM, as in references [6], [7], or [8], is convenient but suffers from a critical limitation: the linear approximation to the motion of a thin plate or beam is valid within only a very small neighborhood of the equilibrium. As transverse motions grow larger, the plate must stretch axially—a geometrically nonlinear deformation that is not present in the linearization of the problem. These effects may become prevalent with deflections as low as 50% of the thickness. For an initially flat panel, axial (or “membrane”) stretching has strong stiffening effects, increasing the stiffness and thus the effective natural frequency of the structure at high amplitudes. For initially curved panels, or panels that are thermally buckled, geometric nonlinearity may also induce snap-through behavior—a potentially catastrophic phenomenon that is exacerbated by external aerodynamic loads. Both of these effects must be well understood to enable the design of robust hypersonic aerostuctures.

Perhaps the most significant phenomenon which results from consideration of geometric nonlinearity is the occurrence of low-amplitude limit cycle oscillations (LCOs) as opposed to the exponential response growth predicted by linear structural theory. This is a well-known behavior observed experimentally [9], analytically [3], [4], [5], and in practice: The Saturn V forward skirt, for example, exhibited low-amplitude flutter during qualification testing with no deleterious effects observed [10]; the A4 missile (later redesignated the V-2 rocket) suffered from sporadic “airburst” failures which were later attributed to panel flutter [11]; and the X-15 experienced widespread panel flutter during initial qualification flights [12], which was solved through an experimental campaign augmented with analytical results [13]. No in-flight failures resulted from X-15 panel flutter; however, inspection of the affected structure did reveal that cracks had initiated at critical locations along the aircraft skin.

Once a structure enters LCO, failure occurs due to fatigue after some period of time, rather than as an immediate catastrophic rupture. The probabilistic nature of fatigue explains the sporadic A4 failures, and the lack of immediate catastrophic failure allowed the X-15 to operate at a panel flutter condition without sustaining catastrophic damage. If nonlinear structural effects are not considered, then panel flutter must be avoided entirely, closing off portions of the flight or design envelope that may in fact be entirely survivable. At a minimum, detailed knowledge of post-flutter behavior allows designers or mission planners to reduce the margin of safety and operate closer to the flutter boundary than would otherwise be advisable.

To capture LCO behavior, geometric nonlinearity may be included in an analysis by simply integrating the full-order equations of motion for a given FEM. Unfortunately, this process is computationally expensive. To consider the effects of geometric nonlinearity without resorting to evaluation of the full FEM, a nonlinear reduced-order model (NLROM) can be used. Several variants of this concept exist, but the type considered in this paper models the nonlinear restoring force as a polynomial in the modal coordinates [14]. This representation requires an upfront construction cost, but once the NLROM is available, dynamic time integrations can be performed with computational costs not much larger than those for a standard linear reduced-order model (ROM). NLROMs have been applied to numerous forced and random vibration problems with good results [15], [16], but their use in the context of flutter analysis is less widespread.

The primary goal of this paper is to demonstrate the successful application of an NLROM derived from a realistic FEM to model postflutter response. Additional concepts are presented as well: for cases in which a structural NLROM is not available, a linearization procedure for third-order piston theory is shown to provide accurate predictions of the asymptotic flutter boundary, commensurate with those obtained via simulation using the nonlinear model. Direct numerical integration of nonlinear piston theory thus provides no benefit for classical flutter boundary computations. However, a final critical point is also noted: nonlinear piston theory can produce amplitude-dependent instabilities that are not predicted by linearization. Such instabilities do not fit naturally within the framework of either classical flutter analysis or traditional post-critical panel flutter analysis, and present an interesting topic for future study.

## A. Motivation

ATA Engineering (ATA) has developed a comprehensive high-fidelity coupled multiphysics simulation framework through various NASA and Air Force Research Laboratory (AFRL) Small Business Innovation Research (SBIR)/Small Business Technology Transfer (STTR) awards. Initial efforts coupled the LOCI/CHEM CFD solver<sup>††</sup> [17] to the Abaqus finite element analysis (FEA) code, using the SIMULIA Co-Simulation Engine<sup>‡‡</sup> as an interface, to perform coupled aeroelastic simulations [18]. An aerothermoelastic (ATE) capability followed shortly after, as demonstrated by Blades et al. [19]. More recent efforts have included ablation modeling in the framework [20], and the module will soon be extended to include detailed simulation of composite material behavior [21] and consideration of servo/actuator mechanics.

In conjunction with AFRL, ATA is currently working toward an ATE validation campaign for this multiphysics framework. The primary objective is to validate a flightlike test article within high-temperature hypersonic flow under quasi-static response conditions, i.e., where deformation of the test article occurs over several minutes and significantly alters aeroheating, surface pressure, and the flow-field shock structure. Secondary objectives include predicting and experimentally observing boundaries where the test article will exhibit nonlinear, dynamic response behavior. ATA is responsible for designing an article and test matrix which will fully exercise the ATE code for validation, introduce as little uncertainty as possible into the results, and, if possible, demonstrate bounded instability at achievable flow conditions. The current target facility for this test is located at the Arnold Engineering Development Center (AEDC). The tunnel of interest provides Mach 4 flow at total pressures in the range of 20 to 100 psi (138 to 689 kPa) and total temperatures ranging from 700 to 1,400 °F (640 to 1,030 K) [22].

The test article design is referred to as the “discovery experiment panel” (DEP). The design is a box panel with an internal crossbar dividing the structure into two unequal bays. The configuration studied in this work is constructed from titanium 6Al-2Sn-4Zr-2Mo (Ti-6242) with all-around thicknesses of 50 mil (1.27 mm), and is bolted to the underlying test fixture along the bottom edges of the panel. The basic configuration of the panel, shown in Figure 1, was influenced by earlier work from Culler and McNamara [3], with the asymmetric two-bay design suggested by Dr. S. Michael Spottswood of AFRL. A key advantage of the stiffened design as opposed to a purely flat panel is that the two-bay model exhibits thermal buckling in relatively low-order modes, whereas a uniform panel displays very high-order buckling shapes that may be difficult to predict accurately or use for validation purposes. To bias the DEP toward a known buckled state, a biasing spring can be added to either the small or the large bay to induce an initial deflection before thermal buckling occurs. Further description of the planned test hardware and objectives can be found in Shah et al. [23].

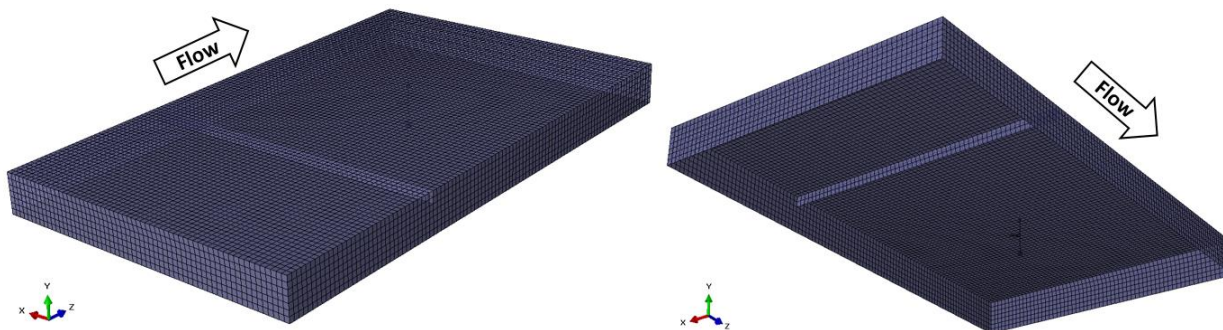


**Figure 1: Geometry and mesh of the discovery experiment panel. The bias spring element is visible in the interior of the large bay.**

To support the design of the test article, ATA has also developed a reduced-order/reduced-fidelity ATE simulation framework using piston theory aerodynamics and Eckert’s reference enthalpy to provide aerodynamic pressure and heating rates to the Abaqus FEM. While the reduced-fidelity framework is computationally efficient enough to analyze a quasi-static ATE response within a matter of minutes, it still requires tens of hours per dynamic analysis—too slow for flutter boundary determination in the design phase. To obtain flutter boundaries within a reasonable amount of

---

<sup>††</sup> LOCI/CHEM is an open-source Navier–Stokes solver developed at Mississippi State University.

<sup>‡‡</sup> Abaqus is a registered trademark of ABAQUS Inc., in the United States and other countries. SIMULIA is a trademark of Dassault Systèmes or its subsidiaries in the United States and other countries.

time, the piston theory aerodynamic approximations were implemented within a MATLAB routine that solves the structural equations of motion in the modal domain so that suitably long time histories can be evaluated in a matter of seconds. Development of this scientific computing framework has enabled the detailed model reduction study presented in this work.

The questions examined here have informed the process of determining flutter boundaries for the DEP for a range of configurations and flow conditions. It must be emphasized that, although the DEP is used as a relevant example, the objective of this paper is a discussion of model reduction methods for flutter detection, and neither the structural design nor the corresponding responses are representative of final hardware or pretest predictions for the validation program as a whole.

For simplicity, this paper focuses primarily on the aerostructural dynamic problem at the initial room-temperature panel state. At the dynamic timescales of interest, it is typically permissible to neglect thermal effects; the thermal problem can be treated in a quasi-static manner which influences only the base state of the dynamic system. To demonstrate the utility of this conceptual framework, a single example of a fully coupled ATE response is examined in part V, section D.

## B. Literature Review

Application of piston theory aerodynamics to flutter problems has a nearly seventy-year history, so only a few recent works most similar to this effort are reviewed here; thorough reviews of panel flutter analysis were conducted by Dowell in 1970 [24], Mei et al. in 1999 [25], and McNamara and Friedmann in 2011 [26]. To further restrict the scope of literature under consideration, works which used a finite element-based structural representation are prioritized over those using analytically derived Galerkin models, which can only be developed for a restricted set of geometries. The ability to model arbitrary structures in a geometrically accurate fashion is critically important for modern design/analysis efforts.

McNamara has extensively studied the hypersonic ATE problem across a wide range of model fidelity levels. Of many possible works, two are highlighted here: a 2010 comparison of various unsteady flow approximations in the hypersonic regime, as applied to a rigid airfoil pitch/plunge model [1], and a 2011 study by Culler and McNamara examining the response of a box panel model [3] in hypersonic flow. The former paper had an objective similar to that of this work, in that it examined the effects of various model forms on flutter boundary predictions, finding that flutter predictions obtained using both second- and third-order piston theory were generally in line with those computed from unsteady CFD. In this paper, instead of varying only the aerodynamic model, various approximations for the structural model are examined as well.

The use of FEM-derived geometrically nonlinear modal models for panel flutter dates back to at least 1994 [27]. To form the NLROM, this and similar work (several more are reviewed in Mei et al. [25]) required access to the internal coding of a nonlinear finite element; such a feature is not available in commercial codes such as Abaqus. Since research-oriented finite element codes are typically not as feature-rich or as extensively validated as their commercial counterparts, this presents a severe limitation on the commercial applicability of the resulting nonlinear models.

An alternative and more recent approach to NLROM generation uses “nonintrusive” methods to construct the nonlinear model based on the inputs and outputs of nonlinear static FEA [16], [14]. Multiple papers authored by Mignolet and others have made extensive use of nonintrusively generated NLROMs for coupled response prediction. Among these, several key works can be sorted by the physical domains considered:

- Dynamic aeroelastic responses in references [28], [29], and [30]
- Unsteady thermoelastic responses in references [31] and [32]
- ATE response in reference [33]

The addition of a reduced thermal basis significantly complicates the process of generating NLROMs, as indicated in the last three works listed above. As such, this work makes no attempt to generate NLROMs that include a thermal basis or the capability to deform with respect to thermal loads. The first three aeroelastic references cited above are quite similar to this paper in terms of the structural modeling approach taken; however, the present work remains distinct in its objective of examining the specific effects of linear/nonlinear structural *and* aerodynamic modeling on flutter and postflutter analysis.

Finally, a study on aeroelastic stability of a cylindrical structure by Klock and Cesnik [7] comprehensively compared flutter predictions using a FEM and a linear modal model, with third-order piston theory applied in both cases to model the aerodynamics. The basis for comparison was a 1967 experimental effort by Olson and Fung [9], which placed a

copper cylinder in Mach 2 flow. Klock and Cesnik found that both the FEM and modal models generally represented the experimental boundary, with the modal model more accurate overall but the FEM better capturing the destabilizing/restabilizing effects of increasing internal pressure. Again, the present inclusion of nonlinear modal models is a key distinction from that past work.

In summary, this work is distinct from those prior through the intersection of two key features:

- Along with the aerodynamic model, consideration is given to the accuracy of the structural model, which is a ROM derived from a geometrically nonlinear FEM.
- The specific items under study are the effects, both qualitative and quantitative, of these different models on flutter boundary predictions.

### C. Organization

The remainder of this paper is organized into five sections. An overview of relevant stability definitions and a brief primer on common stability detection methods is provided in section II. Theoretical development of the aerostructural ROMs is presented in section III. Section IV describes the structural model considered and the flow conditions of interest. In section V, the effects of each model form upon the flutter boundary are examined, along with the influence of each type of model on the predicted domain of attraction and postflutter behavior. Finally, section VI summarizes the work and details some avenues for future investigation.

## II. Stability Properties and Their Determination

### A. Definitions

A few statements on stability of nonlinear systems are given before proceeding. The definitions and terminology used here are taken from Meirovitch [34]. Stability is discussed in the context of an arbitrary nonlinear system with an equilibrium point  $\mathbf{x}_0$ ; departures from this equilibrium are denoted by  $\mathbf{u}$ , with a nonzero initial condition denoted  $\mathbf{u}_0$ . Three relevant definitions are provided:

1. The equilibrium is *stable in the sense of Lyapunov* if for any arbitrary positive  $\epsilon$  and time  $t_0$  there exists a  $\delta > 0$  such that if the inequality

$$\|\mathbf{u}_0\| < \delta$$

is satisfied, then the inequality

$$\|\mathbf{u}(t)\| < \epsilon, t > 0$$

is implied.

2. The equilibrium is *asymptotically stable* if it is Lyapunov stable and, in addition,

$$\lim_{t \rightarrow \infty} \|\mathbf{u}(t)\| = 0$$

The portion of  $\mathbf{u}$  space characterized by the fact that every motion originated in it is asymptotically stable to  $\mathbf{u} = \mathbf{0}$  is called the *domain of attraction* of the equilibrium. If the domain of attraction included the entire  $\mathbf{u}$  space, then the equilibrium is *globally stable*.

3. The equilibrium is *unstable* if for any arbitrarily small  $\delta$  with

$$\|\mathbf{u}_0\| < \delta$$

we have at some finite time  $t_1 > 0$  the situation

$$\|\mathbf{u}(t_1)\| = \epsilon$$

Classical flutter analysis is usually concerned with determining asymptotic stability of the fluid-structural system. Fluttering panels, however, are often stable in the sense of Lyapunov, entering bounded LCO past the flutter boundary rather than failing catastrophically [24]. This behavior is one of the key features of panel flutter and has potential applications for aerospace design: while asymptotic stability is almost universally preferable to Lyapunov stability, it may be possible to intentionally design structures which respond with low-amplitude LCOs during certain high-intensity portions of a given flight envelope. Such a practice could provide designers greater capability to meet mission requirements without sacrificing performance, mass, or cost targets. Lyapunov-stable behavior of the system under study here is discussed in section V, part C.

Additionally, note that asymptotic stability of an equilibrium point does not guarantee global stability of that point. Determining whether a system's domain of attraction is large enough to encompass a structure's reasonable range of

operation can be just as important a task as determining the actual stability of the structure, and it is arguably a more difficult endeavor. The existence of finite domains of attraction for the panel studied in this work is investigated in section V, part D.

## B. Stability Determination: A Priori Methods

Various methods exist to evaluate stability of nonlinear systems in an a priori fashion, but perhaps the two most famous are from Lyapunov. Only the first of these—*Lyapunov’s theorem on stability in the first approximation* or *Lyapunov’s first method*—is applied in this work. (The use of *Lyapunov’s second method* for flutter boundary determination of piston theory systems was demonstrated by Parks [35].) Lyapunov’s first method is described below.

First, suppose one linearizes a system about an equilibrium  $\mathbf{x}_0$  to obtain an approximation of the dynamics in the neighborhood of the equilibrium. The system can be written in first-order form as

$$\dot{\mathbf{z}} = \mathbf{A}_S \mathbf{z} \quad (1)$$

where  $\mathbf{A}_S$  is the time-invariant “state matrix.” Based on its complex eigenvalues, the following statements can be made regarding stability of the *linearized* system:

1. When all the eigenvalues of  $\mathbf{A}_S$  have negative real parts, the system is *asymptotically stable*.
2. When all the eigenvalues of  $\mathbf{A}_S$  have nonpositive real parts but some of the eigenvalues have vanishing real parts, the system is said to possess *critical behavior* and may be either *stable* or *unstable*.
3. If at least one of the eigenvalues of  $\mathbf{A}_S$  has a positive real part, the system is *unstable*.

If either statement (1) or (3) can be made about the system, it is said to possess *significant behavior*. The theorem of Lyapunov’s first method is stated as follows:

*If the variational [linearized] system of equations possesses significant behavior, then the stability characteristics of the linear approximation are the same as for the complete nonlinear equations.*

Unstated in the theorem above is an important qualification: as the linearized equations are valid only in some neighborhood of the equilibrium, stability results obtained using Lyapunov’s first method carry no guarantee of global stability, as the domain of attraction for an equilibrium point cannot be ascertained. Although the linearization approach is a powerful tool for stability analysis, this limitation must be appreciated when applying the technique.

An additional consequence of Lyapunov’s first method is that, in theory, the use of a linearized system for asymptotic stability analysis should be precisely equivalent to the use of the full nonlinear equations of motion about an equilibrium. If a nonlinear system indicates instability where the linear system is stable, this simply indicates that one’s initial conditions have surpassed the domain of attraction of the otherwise stable equilibrium point. Consideration of nonlinear terms is only relevant if one wishes to study more intricate aspects of stability, such as the domains of attraction or existence of LCOs. For this application, more sophisticated techniques are needed; for example, the harmonic balance method can be used to determine LCO amplitude, as demonstrated in Kuo, Morino, and Diugundji [36].

Section V, part A, applies Lyapunov’s first method to determine stability of the system in the neighborhood of its equilibria across a variety of flow conditions.

## C. Stability Determination: A Posteriori Methods

Lyapunov’s first method is only applicable when a linearization of the full system is available; other a priori techniques require the nonlinear equations of motion in closed form. For other cases, such as when CFD or FEA is used to time-integrate the aerostructural equations of motion, stability identification must be performed in an a posteriori fashion by using the integrated response to ascertain the system’s stability properties.

In this work, an eigensystem realization algorithm (ERA) [37] is used to classify the stability of each nonlinear model examined. The ERA applies the same concept as Lyapunov’s first method—that an equivalent linear system can be used to identify the stability of a nonlinear system—but in an inverse manner, by attempting to fit a linear model to a given nonlinear response history. The eigenvalues identified using the ERA determine the system’s stability precisely as described above. Unlike Lyapunov’s first method, which explicitly guarantees that the linearization is an accurate representation in some small neighborhood of the nonlinear system’s equilibrium, it is up to the analyst to provide the ERA with a response that can be represented within the constraints of a linear system.

Stability identification using an ERA is straightforward from a conceptual standpoint, but in practice, it has some disadvantages. Proper identification requires suitable selection of system initial conditions, outputs, and integration times to ensure that the dynamic behavior of interest is sufficiently captured. Certain types of behavior, particularly LCOs, can give misleading results, since such types of response do not fit within the confines of a linear system’s response. In addition to the cost of numerical integration, additional computational cost is incurred from the identification process itself; these procedures must be performed multiple times to locate the flutter boundary in an iterative manner. Finally, stability identification techniques based on equivalent linear systems relate only to asymptotic stability and cannot be used to gain insight into structural LCO.

Despite these shortcomings, a posteriori application of an ERA or a similar technique is the most generally applicable method for identification of coupled numerically integrated nonlinear systems. This fact provides further motivation for the development of closed-form ROMs which can be used to obtain a priori flutter boundaries analytically.

### III. Theoretical Model Development

#### A. Full-Order Co-Simulation

The SIMULIA Co-Simulation Engine provides a capability for multiphysics simulations which leverage Abaqus’ extensive suite of nonlinear structural analysis capabilities. For general analysis of hypersonic structures, the key nonlinearities of interest include temperature-dependent material properties, nonlinear material models, anisotropic materials, detailed radiation models, and geometric nonlinearity. Details of ATA’s work toward full-fidelity simulation of fully coupled hypersonic environments can be found in reference [38]. In the present study, it is only geometric nonlinearity that is of interest. In this context, the aeroelastic equations of motion may be written in the form of the second-order system

$$\mathbf{M}\ddot{\mathbf{x}} + \mathbf{K}(\mathbf{x})\mathbf{x} = \mathbf{f}_{aero}(\mathbf{x}, \dot{\mathbf{x}}; F) \quad (2)$$

with a structural mass matrix  $\mathbf{M}$ , displacement-dependent stiffness matrix  $\mathbf{K}$ , and state-dependent aerodynamic force vector  $\mathbf{f}_{aero}$ , which is also parameterized by a relevant set of flow conditions  $F$ . The vector  $\mathbf{x}$  represents displacement from a zero-stress state, and overdots denote time derivatives. The size of the full-order system is denoted by  $n$ . Damping in the full-order FEM is not considered. In general, viscous damping will delay the onset of flutter, and its neglect can be considered a conservative approximation, although this is not true of all types of damping models [24].

To validate the application of piston theory as a fluid surrogate in hypersonic panel flutter investigations, full-order transient fluid-structure interaction (FSI) simulations of the DEP in a Mach 4 flow were conducted using ATA’s multiphysics framework. The nonlinear structural response of the panel was simulated using Abaqus and the compressible high-speed flow was predicted using LOCI/CHEM. The two solvers are coupled using the SIMULIA Co-Simulation Engine and make up part of the ATA multiphysics framework. The flow domain, shown in Figure 2, contains a rigid wedge panel holder to which the DEP is affixed.

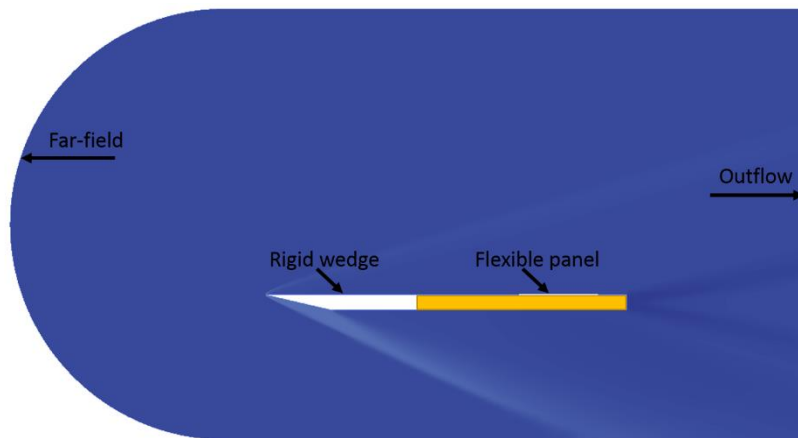


**Figure 2: Side view of the three-dimensional flow domain and summary of boundary conditions for full-order FSI simulations.**

For the flutter boundary study, the freestream temperature and Mach number were fixed at 207.6 K and 4.0, respectively, and the freestream pressure was set to 20 kPa, 30 kPa, and 50 kPa for three separate simulations. The fluid motion was modeled with the compressible unsteady Reynolds-averaged Navier–Stokes (RANS) equations employing the Menter SST turbulence model. The fluid initial condition was established by a steady-state solution of the flow over the wedge and rigid flat panel. The initial condition of the flexible panel was established with the panel biased slightly upward into the flow due to compression of the DEP bias spring. The initial condition for the dynamic FSI simulations was found by finding the steady-state fluid-structure solution of the biased panel in the Mach 4 flow. The dynamic FSI simulations were advanced using a second-order accurate scheme in which the fluid and structure are marched forward in a tightly coupled lockstep, with data transferred at each time step and fluid subiteration. The time step was set to 100  $\mu\text{s}$  to capture all relevant structural timescales. The flutter simulation was initiated by a perturbation to the biased panel in the form of a 1 ms, 100 Pa pressure perturbation on the wetted surface of the panel. As previously discussed, an ERA was used to identify equivalent eigenvalues of the coupled system; the results are compared to piston theory approximations in Figure 4.

## B. Piston Theory Aerodynamics

To reduce the computational cost of the CFD simulation performed above, a variety of unsteady aerodynamic approximation methods are available for hypersonic flows. This work focuses on piston theory, one of the most common and most accurate methods available [1]. Piston theory as an approximation to hypersonic aerodynamics was initially proposed by Lighthill in 1952 [39] and has been applied extensively since that time. The most basic statement of piston theory gives the local unsteady pressure  $p(x, t)$  as a “simple wave” solution based on a local normal velocity  $v_n(x, t)$ , where  $x$  is the horizontal coordinate and  $t$  represents time:

$$\frac{p(x, t)}{p_\infty} = \left[ 1 + \frac{\gamma - 1}{2} \left( \frac{v_n(x, t)}{a_\infty} \right) \right]^{\frac{2\gamma}{\gamma - 1}} \quad (3)$$

The freestream flow quantities are static pressure  $p_\infty$  and speed of sound  $a_\infty$ ; the ratio of specific heats in the fluid is  $\gamma$ . Lighthill showed that a better compromise between the simple wave solution and the potentially more accurate (but more complicated) shock-expansion solution was a third-order expansion of Equation (3):

$$\frac{p(x, t)}{p_\infty} - 1 \cong \gamma \left( \frac{v_n(x, t)}{a_\infty} \right) + \frac{\gamma(\gamma + 1)}{4} \left( \frac{v_n(x, t)}{a_\infty} \right)^2 + \frac{\gamma(\gamma + 1)}{12} \left( \frac{v_n(x, t)}{a_\infty} \right)^3 \quad (4)$$

This “third-order piston theory” is the most commonly recognized form. If only the linear or the quadratic terms in  $v_n$  are retained, one obtains “first-order” or “second-order” variations. There is some question as to whether second-order or third-order expansions are preferable; however, it is well known that the first-order expansion is only valid at angles of incidence extremely close to zero.

Regardless of the evaluation order of the piston theory pressure, the normal velocity is defined as

$$v_n(x, t) = \frac{\partial y(x, t)}{\partial t} + V_\infty \frac{\partial y(x, t)}{\partial x} \quad (5)$$

where  $x$  and  $y$  are the horizontal and vertical spatial coordinates,  $\frac{\partial y(x, t)}{\partial t}$  is the “downwash velocity” resulting from structural motion, and  $V_\infty \frac{\partial y(x, t)}{\partial x}$  is the “incident velocity” resulting from an incidence angle of the structure to the flow. Piston theory is only considered valid when all local normal velocities remain below the freestream speed of sound. Usually, it is a “large” angle of incidence that will cause the approximation to break down; at a freestream Mach number of 4, for instance, an incident angle of just 15 degrees leads to a predicted normal velocity of 1.07 times the speed of sound, invalidating the theory. As such, piston theory is only a valid approximation over portions of a hypersonic vehicle that are nearly parallel to the flow.

Equation (4) can be easily used to apply loading to the surface facets of a FEM on an element-by-element basis. An Abaqus VDLOAD user-defined function (UDF) was written to perform this procedure during an Abaqus/Explicit dynamic analysis, to provide full-order validation of the ROMs based on piston theory aerodynamics. The mathematical representation of this procedure is given by Equation (6).

$$\mathbf{M}\ddot{\mathbf{x}} + \mathbf{K}(\mathbf{x})\mathbf{x} = \mathbf{f}_{piston}(\mathbf{x}, \dot{\mathbf{x}}; F) \quad (6)$$



### C. Vectorized Piston Theory and Aerodynamic Linearization

The first step in moving from full-order representations to ROMs is to introduce the concept of linearization about a base state, which is a feature built into many finite element programs, including Abaqus. This concept is extremely useful: even in a very complicated analysis setting which considers multiple types of nonlinearities, the linearized modes of the structure can be computed at an arbitrary model state to evaluate the dynamic stability or response to small perturbations. The process of base state linearization is equivalent to the first step toward the application of Lyapunov's first method; the resulting linear system can be used to assess stability of the nonlinear equilibrium point. Once a model has been linearized about a displacement state  $\mathbf{x}_0$ , the resulting equation of motion is written

$$\mathbf{M}\ddot{\mathbf{u}} + \mathbf{K}(\mathbf{x}_0)\mathbf{u} = \mathbf{f}_{piston}(\mathbf{u}, \dot{\mathbf{u}}; F) \quad (7)$$

with departures  $\mathbf{u}$  from the equilibrium displacement. The piston theory expressions to follow are written in terms of this perturbed displacement. It should be understood that the piston theory force itself is also modified to correspond to the base state linearization; the base state aerodynamic force must be subtracted from the right-hand side of the system to maintain equilibrium. All linearizations are performed from a static equilibrium obtained using piston theory aerodynamic forces rather than those obtained from CFD.

The normal velocity in Equation (5) hides several nonlinearities within its definition. For efficiency of numerical integration within scientific computing environments such as MATLAB or Python, the normal velocity<sup>§§</sup> at each element can be linearized and written in a vectorized form as

$$\mathbf{v}_n = M_\infty \boldsymbol{\theta}_0 + M_\infty \mathbf{A}\mathbf{u} + \frac{1}{a_\infty} \mathbf{B}\dot{\mathbf{u}} = \mathbf{v}_0 + \mathbf{v}_e \quad (8)$$

where the initial incident velocity,  $\mathbf{v}_0 = M_\infty \boldsymbol{\theta}_0$ , depends on an array of initial incident facet angles in  $\boldsymbol{\theta}_0$ . An array of pressure ratios can be represented using the function  $\mathbf{c}_p(\mathbf{v}_n; F)$ . These pressure ratios can be premultiplied by an aerodynamic influence matrix  $\mathbf{D}$ , which is constructed by considering the element normal vectors and areas to obtain  $\mathbf{f}_{aero} = p_\infty \mathbf{D}\mathbf{c}_p(\mathbf{v}_n; F)$  for a given choice of aerodynamic pressure function.

When third-order piston theory is used to provide the aerodynamic pressures, the full-order linearized system becomes

$$\mathbf{M}\ddot{\mathbf{u}} + \mathbf{K}(\mathbf{x}_0)\mathbf{u} = p_\infty \gamma \mathbf{D} \left\{ \mathbf{v}_n \circ \left[ \mathbf{1} + \frac{\gamma+1}{4} \mathbf{v}_n \circ \left( \mathbf{1} + \frac{1}{3} \mathbf{v}_n \right) \right] - \mathbf{v}_0 \circ \left[ \mathbf{1} + \frac{\gamma+1}{4} \mathbf{v}_0 \circ \left( \mathbf{1} + \frac{1}{3} \mathbf{v}_0 \right) \right] \right\} \quad (9)$$

with the  $(\circ)$  operator denoting the Hadamard (elementwise) product and  $\mathbf{1}$  denoting an appropriately sized vector of ones. The nonlinear force at equilibrium corresponding to the equilibrium normal velocity array  $\mathbf{v}_0$  is subtracted from the right-hand side of the equation to reflect that these forces are built into the equilibrium equations of motion.

Though the structural expression is linear, the aerodynamic forces remain nonlinear. If the right-hand side of the equation is linearized, stability of the system can be calculated directly by evaluating the eigenvalues of the corresponding first-order state matrix. Linearizing Equation (9) with respect to the perturbation states results in

$$\mathbf{M}\ddot{\mathbf{u}} + \mathbf{K}(\mathbf{x}_0)\mathbf{u} = p_\infty \gamma \mathbf{D} \left[ \mathbf{I} + \frac{\gamma+1}{2} \mathbf{V}_0 \left( \mathbf{I} + \frac{1}{2} \mathbf{V}_0 \right) \right] \left[ M_\infty \mathbf{A}\mathbf{u} + \frac{1}{a_\infty} \mathbf{B}\dot{\mathbf{u}} \right] \quad (10)$$

To maintain a matrix form of the equations with respect to the perturbations in  $\mathbf{v}_e$ , the identity matrix  $\mathbf{I}$  and a diagonal matrix  $\mathbf{V}_0 = \text{diag}(\mathbf{v}_0)$  are used in Equation (10). Contrast this with the expression for first-order piston theory, which results in a linear system with no further modification:

$$\mathbf{M}\ddot{\mathbf{u}} + \mathbf{K}(\mathbf{x}_0)\mathbf{u} = p_\infty \gamma \mathbf{D} \left[ M_\infty \mathbf{A}\mathbf{u} + \frac{1}{a_\infty} \mathbf{B}\dot{\mathbf{u}} \right] \quad (11)$$

This linearization procedure was first described in 1962 [40] and has been implemented in at least one commercial aeroelasticity code (Nastran, as described in reference [41]). However, the use of linearized third-order piston theory is not apparent in recent literature on the topic of hypersonic aeroelasticity. Further investigations toward the utility of the linearization procedure in flutter boundary prediction were performed in reference [42]. As seen below, the linearized expressions are entirely sufficient for predicting the same asymptotic flutter boundary as nonlinear piston theory.

---

<sup>§§</sup> In an abuse of nomenclature, the ‘‘normal velocities’’ in Equation (8) are actually normalized with respect to  $a_\infty$ , simplifying the resulting expression for piston theory pressures.

## D. Modal Reduction

Once the aerodynamics can be evaluated quickly, the structural problem becomes a bottleneck: While linearization of the structure greatly reduces the computational cost associated with model assembly and iterative solution procedures, the cost of a linear solution for a large structure is still quite high due to the small time steps and large solution costs associated with such models. A modal reduction dramatically lowers the order of the equations of motion by specifying  $\mathbf{u} = \mathbf{\Phi}\mathbf{q}$ , with the size  $n \times m$  modal matrix  $\mathbf{\Phi}$  transforming the  $m$  modal coordinates  $\mathbf{q}$  to physical displacements (for a useful reduction,  $m \ll n$ ). The modal matrix is determined via solution of the generalized eigenvalue problem,

$$[\mathbf{K}(\mathbf{x}_0) - \omega_i^2 \mathbf{M}] \boldsymbol{\phi}_i = \mathbf{0} \quad (12)$$

where  $\mathbf{\Phi} = [\boldsymbol{\phi}_1 \ \boldsymbol{\phi}_2 \ \cdots \ \boldsymbol{\phi}_m]$  is normalized such that  $\mathbf{\Phi}^T \mathbf{M} \mathbf{\Phi} = \mathbf{I}$  and  $\mathbf{\Phi}^T \mathbf{K}(\mathbf{x}_0) \mathbf{\Phi} = \boldsymbol{\Lambda}(\mathbf{x}_0)$ . The inner product through the stiffness matrix is diagonal, with  $\Lambda_{ii} = \omega_i^2$ . To introduce damping into the system, a damping matrix  $\mathbf{Z}$  can be introduced, with  $Z_{ii} = 2\zeta_i \omega_i$  along each diagonal entry. The damping ratio  $\zeta_i$  can either be measured from dynamic test or estimated as a value on the order of one percent. In this work, no consideration is given to damping in the structure.

An alternative modal reduction can be obtained by including the linear aerodynamic contributions to damping and stiffness in the eigenvalue problem. However, these matrices are not, in general, symmetric; as a result, the classical modal decomposition shown above is not applicable. This feature of the system can be treated by casting the system into state-space form and performing a non-obvious rearrangement of the left and right eigenvectors, as shown by Patil [43]. This approach was applied to the present problem in reference [42] but is beyond the scope of this paper; only the classical modal reduction is considered here.

Depending on the form of the aerodynamic forcing selected, two types of ROMs using linear structural representations can be written:

$$\ddot{\mathbf{q}} + \boldsymbol{\Lambda}(\mathbf{x}_0)\mathbf{q} = p_\infty \gamma \mathbf{\Phi}^T \mathbf{D} \left\{ \mathbf{v}_n \circ \left[ \mathbf{1} + \frac{\gamma+1}{4} \mathbf{v}_n \circ \left( \mathbf{1} + \frac{1}{3} \mathbf{v}_n \right) \right] - \mathbf{v}_0 \circ \left[ \mathbf{1} + \frac{\gamma+1}{4} \mathbf{v}_0 \circ \left( \mathbf{1} + \frac{1}{3} \mathbf{v}_0 \right) \right] \right\} \quad (13a)$$

$$\ddot{\mathbf{q}} + \boldsymbol{\Lambda}(\mathbf{x}_0)\mathbf{q} = p_\infty \gamma \mathbf{\Phi}^T \mathbf{D} \left[ \mathbf{I} + \frac{\gamma+1}{2} \mathbf{V}_0 \left( \mathbf{I} + \frac{1}{2} \mathbf{V}_0 \right) \right] \left[ M_\infty \mathbf{A} \mathbf{\Phi} \mathbf{q} + \frac{1}{a_\infty} \mathbf{B} \mathbf{\Phi} \dot{\mathbf{q}} \right] \quad (13b)$$

In Equation (13a), the use of the modal states  $\mathbf{q}$  and  $\dot{\mathbf{q}}$  is implicit, whereas their inclusion in Equation (13b) is explicit.

## E. Nonlinear Reduced-Order Models

For thin plate and beam structures, assumptions of linearity begin to break down once displacements as low as 50% of the thickness are achieved. At full order, the linearized restoring force  $\mathbf{K}(\mathbf{x}_0)\mathbf{u}$  may be augmented by a nonlinear function of the displacements  $\mathbf{f}_{nl}(\mathbf{u})$ . Explicitly describing such a function in the full-order FEM is not practical, but in the reduced modal space, a vector function  $\boldsymbol{\theta}(\mathbf{q})$  can be represented as a polynomial in the modal coordinates, with the  $r^{th}$  term given by

$$\theta_r(q) = \sum_{i=1}^m \sum_{j=1}^m A_{r,ij} q_i q_j + \sum_{i=1}^m \sum_{j=1}^m \sum_{k=1}^m B_{r,ijk} q_i q_j q_k \quad (14)$$

The coefficients of this function are specified using a series of nonlinear static finite element solutions, as detailed in reference [44]. The number of static load cases required to specify the NLROM grows with either the cube or the square of modes in the basis, depending on the identification method selected. For models including just a few modes (i.e., fewer than ten), the construction costs are trivial compared to even a single time integration of the full-order equation of motion.

The resulting nonlinear modal equation of motion is a simple modification of Equation (13a):

$$\ddot{\mathbf{q}} + \boldsymbol{\Lambda}(\mathbf{x}_0)\mathbf{q} + \boldsymbol{\theta}(\mathbf{q}) = p_\infty \gamma \mathbf{\Phi}^T \mathbf{D} \left\{ \mathbf{v}_n \circ \left[ \mathbf{1} + \frac{\gamma+1}{4} \mathbf{v}_n \circ \left( \mathbf{1} + \frac{1}{3} \mathbf{v}_n \right) \right] - \mathbf{v}_0 \circ \left[ \mathbf{1} + \frac{\gamma+1}{4} \mathbf{v}_0 \circ \left( \mathbf{1} + \frac{1}{3} \mathbf{v}_0 \right) \right] \right\} \quad (15)$$

While linearized piston theory could also be used in conjunction with a structural NLROM, such an approach offers little practical benefit since the equations of motion must still be numerically integrated due to the presence of a nonlinear restoring force. To reduce the number of comparisons necessary in the results below, only the model form using both nonlinear structural and aerodynamic terms is considered.

## F. Consolidation

The various numerical models under consideration are presented in Table 1 and summarized in the list below.

- **Abaqus/CFD:** Full-order evaluation of the nonlinear structural model with the SIMULIA Co-Simulation Engine used to couple time-accurate CFD results to structural deformations and velocities. Costly evaluation (tens of hours wallclock time/thousands of hours CPU time); infeasible for flutter boundary prediction. Dynamic integration of the FEM was conducted using the Abaqus/Standard implicit code, which is unconditionally stable and allowed the use of a relatively large time increment of 100  $\mu$ s to minimize the required number of CFD evaluations.
- **Abaqus/UDF:** Full-order explicit dynamic evaluation of the nonlinear structural model with piston theory aerodynamics computed on an element-by-element basis via a user-defined subroutine. Moderately costly evaluation (tens of minutes); unwieldy for flutter boundary prediction. In this case, dynamic integration of the FEM was performed using the conditionally stable Abaqus/Explicit code, which is computationally efficient on a per-time-step basis but requires extremely small time steps on the order of 100 ns to maintain computational stability.
- **L-3P:** Linear structure; third-order piston theory. Time histories simulated by numerical integration, with flutter boundary located iteratively based on multiple numerical integrations. Efficient evaluation (tens of seconds) and low boundary prediction cost (several minutes). This model was integrated using the trapezoidal Newmark- $\beta$  method with zero numerical damping and a fixed time increment of 500  $\mu$ s.
- **L-LP:** Linear structure; linearized (third-order) piston theory. Unforced time histories available in closed form and boundary prediction based on eigensolutions of the modal system matrices (negligible cost for low-order modal models.) Where necessary, time responses were obtained using MATLAB's `lsim` procedure, which uses analytical relations to obtain the response of linear systems.
- **NL-3P:** Nonlinear structure; third-order piston theory. Building a structural NLRM using Equation (14) requires hundreds or thousands of nonlinear static procedures which may take minutes or hours to compute. Once the NLRM is computed, time histories and flutter boundaries are simulated/located numerically as in the L-3P case, in a matter of seconds/minutes using the same integration scheme as the L-3P model.

**Table 1: List of numerical models for computation of flutter and postflutter panel behavior.**

Description	Designation	Eq. No.	Rough Wallclock Time per Integration [s]
Full-order FEM coupled to CFD	Abaqus/CFD	(2)	$10^5$
Full-order FEM coupled to nonlinear piston theory	Abaqus/UDF	(3)	$10^3$
Linear ROM; nonlinear piston theory	L-3P	(13a)	$10^0$
Linear ROM; linearized piston theory	L-LP	(13b)	$10^{-1}$
NLRM; nonlinear piston theory	NL-3P	(15)	$10^0$

Integration times presented in Table 1 are approximate and intended for reference only; the actual computational cost of integration will depend upon model size, period of integration, and number of modes retained in the ROMs. Note that the Abaqus/CFD computations were carried out using 1,100 CPUs for CFD computation and a single CPU for the Abaqus FEA calculations. While aerodynamic calculations accounted for the vast majority of CPU time, the ability of CFD codes to scale very well in parallel computations meant that the structural calculations accounted for 80% of wallclock time. Even assuming a very generous factor of 10 speedup in the Abaqus calculations with the structural computations performed in parallel, one should expect the structural portion of this problem to account for roughly a third of the wallclock time, with that proportion increasing as further CPUs are made available for the CFD solver.

## IV. Structural Model and Flow Conditions

### A. Description

The structural test article of interest is a two-bay box panel loosely based on a previous numerical study performed by Culler and McNamara [3]. This specific configuration was proposed initially by Dr. S. Michael Spottswood of AFRL. Leaving aside the specifics of attachment to the tunnel apparatus, the panel is 12 inches by 20 inches in dimension with a height of 1.5 inches. A 0.5 inch cross-rib is located one-third of the way down the panel, with the smaller of the two bays oriented in the direction of incoming flow. The nominal panel thickness is 50 mils (1.27 mm), and the current material selection is Ti-6242 alloy. The geometry and mesh are shown in Figure 1.

Once the panel temperature increases by 50–100 °F, both bays of the panel enter a buckled state; these temperatures occur within seconds of tunnel entry. Preliminary simulations indicated that the global buckling of the panel was unpredictably influenced by various model parameters and would likely be dominated by manufacturing imperfections in the physical test article. To provide a predictable buckled state for co-simulation verification, certain versions of the design included a bias spring added to the interior of the large bay, providing a slight upward force at room temperature. The spring used for this work has a rate of 10 pounds per inch and, when the panel is perfectly flat, an initial compression of 0.5 inch. In all simulations, the panel first comes to its static equilibrium before the flow is activated in a follow-on step.

The finite element mesh consisted of 8,788 nodes and 8,626 four-node reduced integration shell elements (S4R in Abaqus nomenclature). Only the 6,222 elements on the top panel surface are included in the aerodynamic calculation. For aeroelastic simulations, the “general shell section” property was used to specify shell element behavior, and the more computationally intensive through-thickness integration process, with three points per node, was used for the ATE test case. The panel boundary is fully fixed at each node along the bottom edge of the side walls; the grounding node of the bias spring is also fully fixed.

For the linear ROMs (L-3P and L-LP), the first twenty normal modes of the panel were retained in the equations of motion. Not all of these modes are equally important to modeling the aeroelastic behavior of the panel; after initial study, a smaller set of five modes were selected for the NLROM, to minimize the construction time of the nonlinear model. For the linear ROM, modes computed at the bias spring equilibrium position were used to represent the structural deformation; for the NLROM, modes at the undeformed state were used. As a result, the NLROM was equilibrated to the bias spring in a reduced modal space, which reduced the accuracy of its initial displacement location (no residual mode was included in the NLROM to represent deflections due to the bias spring.) While this leads to a noticeable offset of the NL-3P time histories relative to the other models, its dynamics were only marginally affected. Further details on the selection of these modes and construction of the NLROM are presented in the appendix.

### B. Flow Conditions

The target facility for DEP testing is a Mach 4 continuous-flow tunnel with high-temperature flow capabilities. At Mach 4, true pressure/temperature curves corresponding to standard atmosphere tables can be maintained up to at least 130,000 feet; more severe conditions are also available up to a maximum total pressure  $p_T$  of 100 psi (689 kPa) and total temperature  $T_T$  of 1,400 °F (1030 K). Under thermally perfect assumptions (an ideal gas with no variation in specific heats as a function of temperature), total conditions (or “stagnation” conditions) are related to the static freestream conditions as

$$\frac{T_T}{T_\infty} = \left(1 + \frac{\gamma - 1}{2} M_\infty^2\right) \quad (16)$$

$$\frac{p_T}{p_\infty} = \left(\frac{T_T}{T_\infty}\right)^{\frac{\gamma}{\gamma-1}} \quad (17)$$

The baseline flow condition for the bulk of DEP analysis work has been a 70,000 foot true pressure/temperature condition, with  $p_T = 100$  psi (689 kPa) and  $T_T = 1,100$  °F (870 K). As shown below, there is no risk of unheated panel flutter at these conditions. For the remainder of this paper, the baseline pressure is adjusted to a static value of  $p_\infty = 20$  kPa. The baseline temperature conditions remain unchanged but enter the analysis only through the freestream speed of sound  $a_\infty = 288.8$  m/s. The baseline Mach number also remains  $M_\infty = 4$  and, for air, the standard specific heat ratio  $\gamma = 1.4$  is used.

### C. Representative Time Integration

To verify the correctness of each model form involving piston theory, the last four model types in Table 1 were integrated over a period of 0.25 second for comparison. The Abaqus model was linearized at the baseline flow condition using a 20 kPa static pressure; for the dynamic simulation, the freestream static pressure was instantaneously adjusted to 30 kPa to induce a response. The resulting displacement time histories are shown in Figure 3, with the response of the large bay midpoint shown. All displacement plots to follow track the large bay midpoint displacement as well.

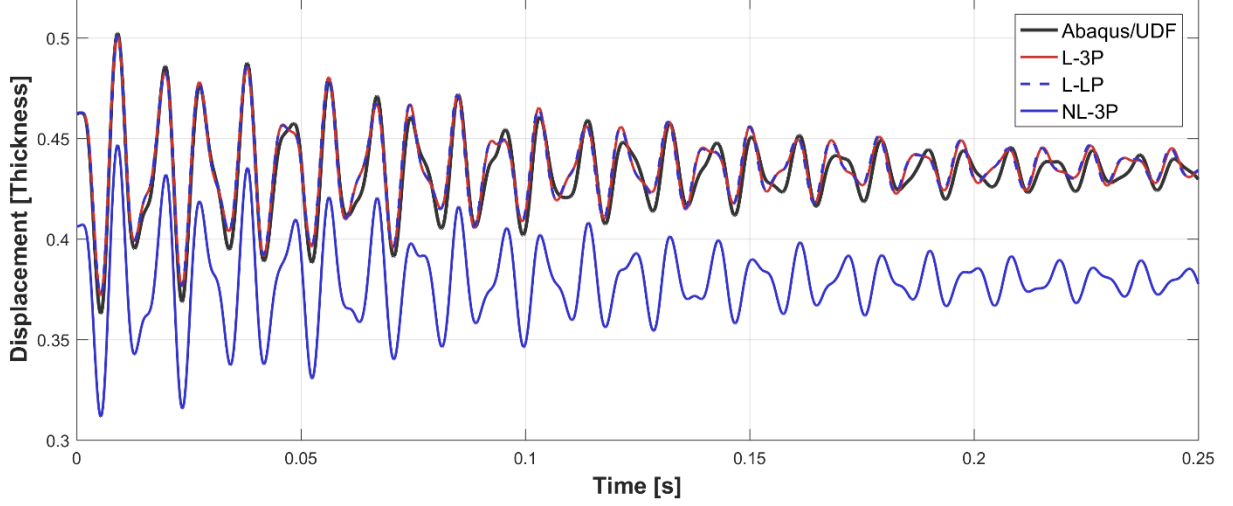


**Figure 3: Representative time integration of a dynamic response using all four piston-theory-based models in Table 1. The displacement response of the DEP large bay midpoint is depicted. Solutions initiated from the 20 kPa equilibrium point after a step change in freestream pressure to 30 kPa.**

Both the L-LP and L-3P variants, using linear structural models, match the Abaqus results almost precisely over the entire time history—clearly, nonlinear structural effects are not important for this particular response. As discussed above, the NL-3P model has an initial offset and, since it includes only five basis vectors, yields a somewhat different response than the other models. The overall dynamics remain similar, however.

The Abaqus/CFD response does not bear a strong resemblance to the piston theory approximations in terms of a time history. The dynamic characteristics of this model are compared to its piston theory counterparts below.

## V. Stability Boundary Effects

### A. Linear Flutter Boundary

For the case of the linearized L-LP system, flutter onset can be determined by converting the second-order Equation (13b) to a first-order system. Rewriting Equation (13b) in continuous time state-space notation per the form of Equation (1) results in

$$\begin{Bmatrix} \dot{\mathbf{q}} \\ \ddot{\mathbf{q}} \end{Bmatrix} = \begin{bmatrix} \mathbf{0}_{mm} & \mathbf{I}_{mm} \\ -\mathbf{\Lambda} + \bar{\mathbf{K}} & \bar{\mathbf{C}} \end{bmatrix} \begin{Bmatrix} \mathbf{q} \\ \dot{\mathbf{q}} \end{Bmatrix} \quad (18)$$

Eigenvalues of the state matrix  $\mathbf{A}_S$  determine stability of the system. The two additional matrices used above are the reduced aerodynamic stiffness  $\bar{\mathbf{K}}$  and reduced aerodynamic damping  $\bar{\mathbf{C}}$ .

$$\bar{\mathbf{K}} = p_\infty M_\infty \gamma \Phi^T \mathbf{D} \left[ 1 + \frac{\gamma + 1}{2} \mathbf{V}_0 \left( 1 + \frac{1}{2} \mathbf{V}_0 \right) \right] \mathbf{A} \Phi \quad (19)$$

$$\bar{\mathbf{C}} = \frac{p_\infty \gamma}{a_\infty} \Phi^T \mathbf{D} \left[ 1 + \frac{\gamma + 1}{2} \mathbf{V}_0 \left( 1 + \frac{1}{2} \mathbf{V}_0 \right) \right] \mathbf{B} \Phi \quad (20)$$

For the remaining model forms, dynamic characteristics were identified a posteriori using an ERA, as discussed in section II part C. The algorithm was instructed to identify four dominant modes from the response, based on the displacement time histories from the midpoint of the panel's large and small bay.

## B. Boundary Comparisons

First, the level of agreement between CFD and piston theory is assessed. Responses from ten Abaqus/UDF and three Abaqus/CFD simulations were used to plot identified frequencies and damping ratios as a function of static pressure. To better understand the structure of the results, a large number of L-LP frequency and damping results were also computed to form a set of continuous frequency/damping curves across the pressure sweep. The identified system properties are shown in Figure 4.

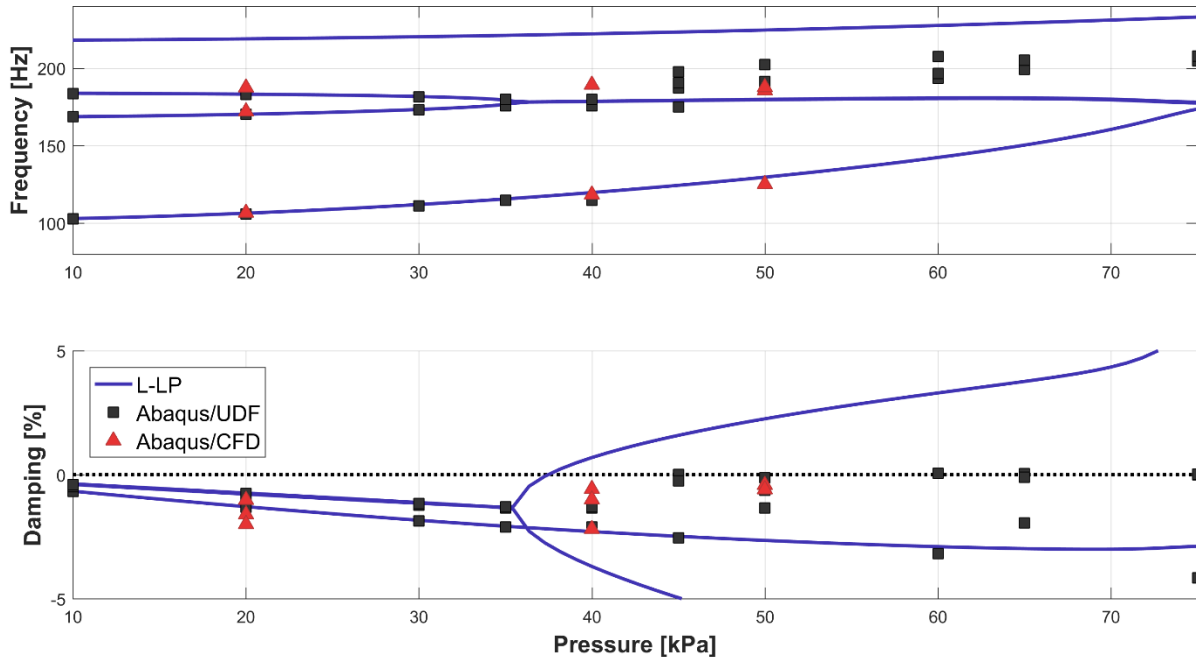


**Figure 4: Linearized L-LP frequency (top) and damping ratio (bottom) as a function of static pressure, along with results corresponding to ten Abaqus/UDF and three Abaqus/CFD simulations.**

Agreement between CFD and piston theory is not particularly good in this case. The L-LP model predicts a flutter boundary of 37.5 kPa, whereas the Abaqus/UDF boundary lies somewhere between 40 and 45 kPa. However, the Abaqus/CFD model did not flutter at 50 kPa, although a clear upward trend in the identified damping ratios is observable. Sufficient computer time to run a 60 kPa Abaqus/CFD co-simulation could not be obtained in time for submission of the paper.

On the other hand, the piston theory model does accurately represent the convergence of modes 2 and 3, which is observable in all three model forms plotted above. The disagreement between piston theory and CFD in this case is likely due to three-dimensional effects on the panel, which cause flow to spill outward and produce unmodeled forces on the panel surface that cannot be predicted by piston theory aerodynamics. The objectives of the paper are not largely influenced by these effects: piston theory is intended to be used as an approximation, and, to the extent that it is able to quickly predict conservative flutter boundaries for the DEP, it remains a useful model.

With an evaluation of piston theory for this problem complete, the various model forms can be compared. The L-3P and NL-3P models were evaluated at 100 pressure locations; the identified frequency and damping values are shown in Figure 5. The Abaqus/UDF and L-LP system properties are retained, although the Abaqus/CFD results are removed.

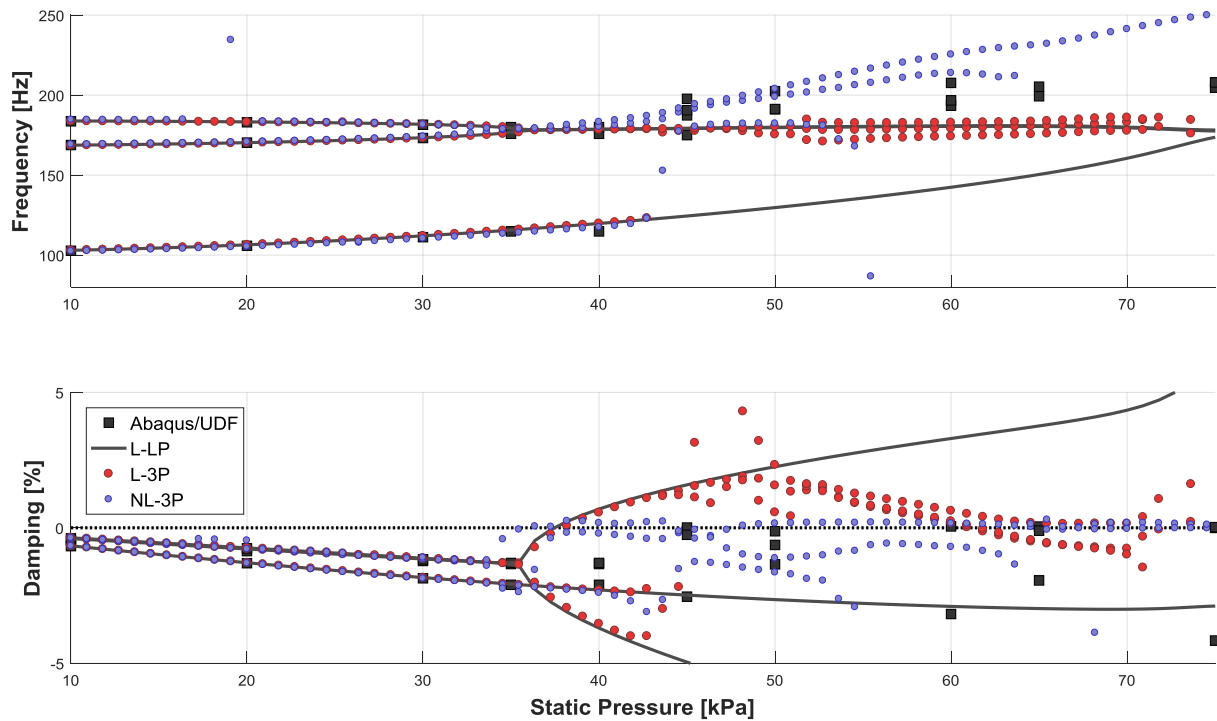


**Figure 5: Frequency (top) and damping (bottom) behavior vs. static pressure. The L-3P, L-LP, and NL-3P results align almost perfectly until well beyond the asymptotic flutter boundary.**

Below the asymptotic flutter boundary, all three reduced model forms agree almost precisely. The only notable discrepancy comes from the NL-3P model; as discussed, this model only uses five structural modes and yields a somewhat lower flutter boundary as a result. As expected from Lyapunov’s first theorem, the linearized model possesses the same asymptotic stability characteristics as the nonlinear systems.

Past the flutter boundary, the properties diverge. Since the ERA is attempting to fit nonlinear responses within the framework of linear systems, the results are of only limited value; however, it is evident that the L-3P behaves in a fashion more similar to the linear system over a greater region of the pressure range. In particular, the identified frequencies stay relatively constant, and the damping ratios continue to track the L-LP branch until roughly 50 kPa. The Abaqus/UDF and NL-3P results, on the other hand, indicate a slight climb in identified frequency along with a near-zero damping ratio past the flutter boundary. The near-zero damping ratio is indicative of an LCO since the ERA interprets the constant-amplitude oscillation as an undamped mode.

### C. Postcritical Behavior

As expected, nonlinear model forms provided no useful information toward determination of the flutter boundary when compared to the fully linearized L-LP system. Postcritical behavior is an entirely different matter. Abaqus/UDF, L-3P, and NL-3P time histories computed using static pressures of 30, 50, 60, and 75 kPa are compared in Figure 6. The L-LP model is omitted, as it performs identically to the nonlinear model forms for the stable 30 kPa case but exponentially diverges for the three postcritical cases, obscuring the other results.

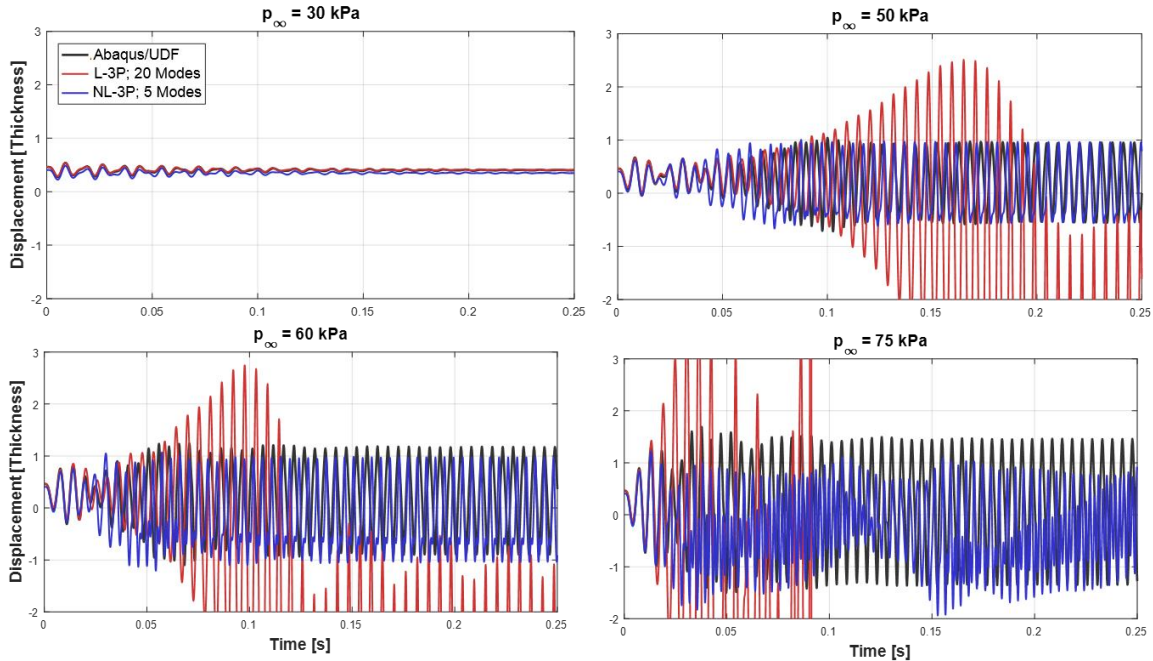


**Figure 6: Comparison of Abaqus, L-3P, and NL-3P results over a 0.25 second simulation window at a stable static pressure of 30 kPa and three postflutter static pressures of 50, 60, and 75 kPa.**

The Abaqus/UDF model enters a stable, fairly regular LCO which increases in amplitude as the pressure rises. At 50 kPa, the NL-3P model matches this response quite well; as the pressure increases above 60 kPa, the agreement deteriorates, appearing quite poor at 75 kPa. The L-3P model, on the other hand, disagrees entirely in the postflutter region. The structural response is far too large, and while the nonlinear aerodynamic terms do lead to an LCO, its amplitude and mean value are significantly different from the actual LCO equilibrium. At 75 kPa, the L-3P integration fails entirely, due to the large oscillation levels of the system. In this case, including nonlinear piston theory without also adding in a nonlinear panel model is not worth the extra computational cost of nonlinear integration and system identification.

A more systematic comparison of the NL-3P model's effectiveness was performed in an ad hoc manner by computing the root mean square (RMS) response of the latter half of each postflutter time history from the Abaqus/UDF and NL-3P results and scaling by a factor of  $\sqrt{2}$  to estimate the peak displacement level of the LCO. LCO frequency estimates were obtained by performing a Fourier transform of the same portion of the time history and noting the frequency that corresponded to the peak Fourier coefficient. The results of this procedure are shown in Figure 7.



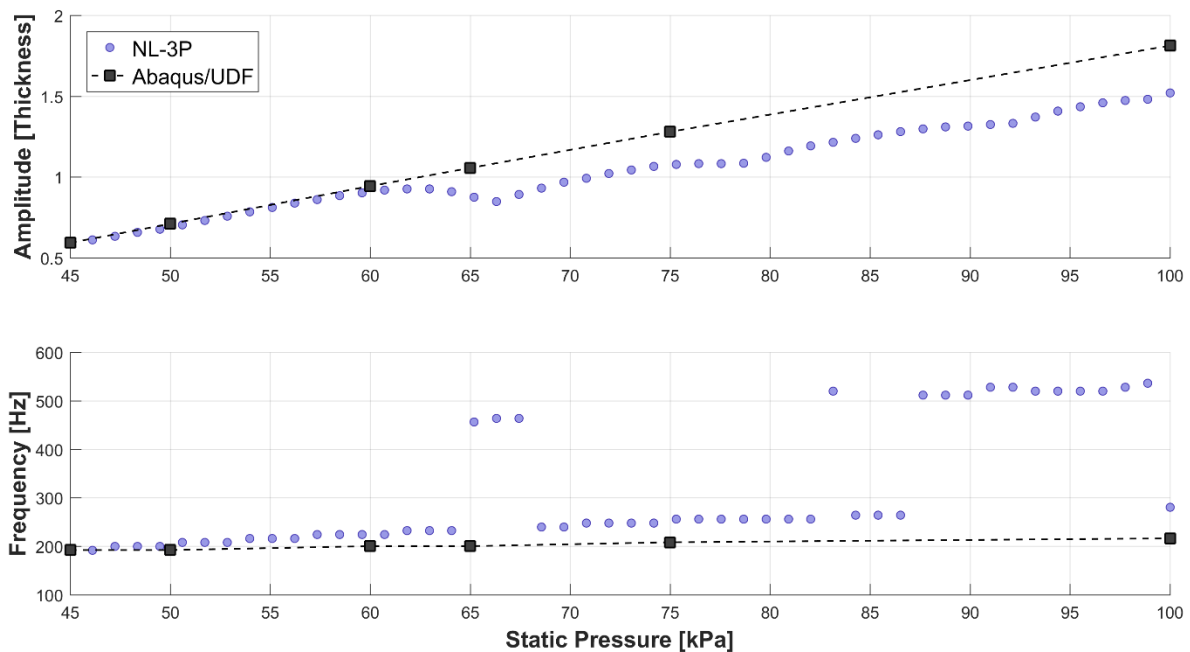


**Figure 7: Ad hoc comparison of LCO amplitude (top) and frequency (bottom) between the NL-3P and Abaqus/UDF models.**

As demonstrated in Figure 6, the models agree fairly well up to roughly 60 kPa, a pressure 60% larger than the L-LP asymptotic flutter boundary (though only 40% larger than the Abaqus/UDF flutter boundary). Beyond this level, the amplitude predictions remain somewhat accurate, although the LCO frequencies become much less reliable, jumping between the mode 2/3 value near 200 Hz and a spurious 500 Hz frequency; this additional high-frequency component of the response is also observable in the 75 kPa result of Figure 6.

These discrepancies aside, the NLROM dramatically increases the post-flutter accuracy of the ROM, providing the only model form in which it can accurately and efficiently perform calculations beyond the flutter boundary. It is likely that an NLROM tuned to provide accurate responses at higher displacements, or constructed with additional basis vectors, could match the full-order model up to even higher pressure levels.

#### D. Aerothermoelastic Application

Results presented to this point have focused only on the aeroelastic panel response. In practice, it is the ATE response that is of interest. Before concluding, a long-term dynamic ATE response is shown, and the utility of the L-LP linearization method is further demonstrated. An intriguing feature of the nonlinear aerodynamic response is also highlighted.

It must be again emphasized that the ATE time history shown here will not be representative of an actual DEP test. In fact, the panel thickness in this case was switched from the nominal 50 mils (1.27 mm) to a thinner value of 30 mils (0.762 mils). The reduced-thickness panel is of academic interest due to its reduced stability margin but of no practical interest as it cannot actually be machined using the desired processes.

The thermal timescale of the thin panel is significantly smaller than that of its thicker counterpart, so a dynamic simulation can feasibly be performed over a roughly ten-second period of transient thermal heating, by which point the panel begins to approach a steady-state temperature. Dynamic coupled temperature-displacement simulations in Abaqus can only be performed using the explicit code, which requires a very small time step (on the order of 100 ns) due to its conditional stability. The use of CFD for computation of aerothermal loads is impractical over the time periods of interest. Instead, the piston theory aerodynamic approximation was coupled to Eckert's reference enthalpy method [2] to obtain representative heating loads, which were coupled to the surface pressure distribution obtained from piston theory. Due to the added complexity of the reference enthalpy method, the SIMULIA Co-Simulation Engine was used for the additional physics, rather than Abaqus user-defined functions. The dynamic simulation was

carried out over a period of ten seconds, with a 1,100 °F (870 K) stagnation temperature and 100 psi (690 kPa) total pressure specified. Over the course of the simulation, the panel temperature shifts from an initial room-temperature value to an eventual average of roughly 800 °F (700 K). The quasi-static displacement of the panel shifts from a mean displacement of two thicknesses to roughly twelve thicknesses over the same period of time. Temperature-dependent material properties were used for this simulation, with the most relevant effect being a large reduction in elastic modulus at high temperatures.

In addition to the dynamic simulation, a quasi-static coupled temperature-displacement solution was also computed. Both the dynamic and quasi-static responses are shown in the upper pane of Figure 8. To assess the performance of the L-LP linearization procedure, each converged increment of the quasi-static solution was used to compute structural modes, aerodynamic influence matrices, and the resulting system frequencies and damping ratios. The maximum damping ratio at each increment is plotted as a function of time in the lower pane of Figure 8.

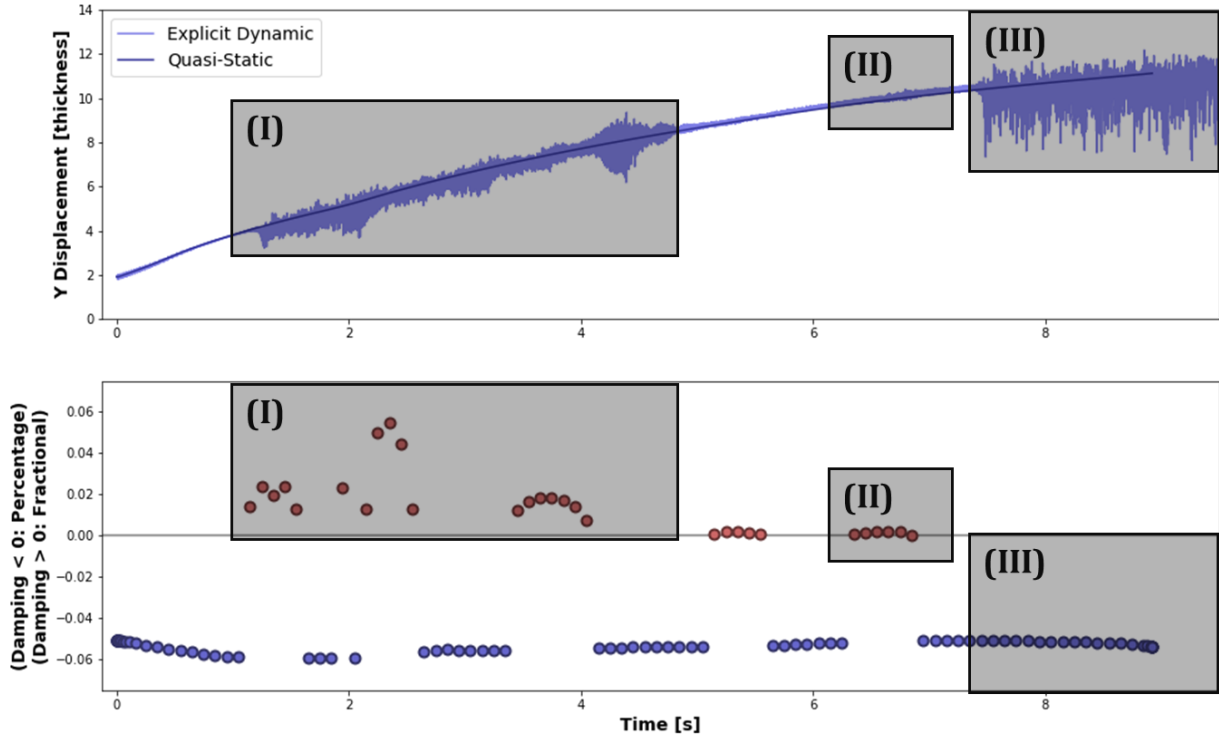


**Figure 8: (Top): Dynamic and quasi-static coupled temperature displacement ATE solutions over a period of ten seconds. (Bottom): Maximum damping ratio for each converged increment of the quasi-static solution, computed using the L-LP linearization methodology.**

The quasi-static solution tracks the backbone of the explicit dynamic solution but gives no indication of the varying stability characteristic of the panel as temperature increases. At roughly eight seconds, the panel enters a high-amplitude LCO; at nine seconds, the quasi-static simulation fails due to a singular stiffness matrix, which denotes a condition of zero natural frequency. The final dynamic instability is likely caused by this reduction in natural frequency, but LCO onset significantly precedes the quasi-static failure point.

Three zones of interest are highlighted for comparing the dynamic results to the L-LP damping predictions. In zone I, a large number of unstable damping points are matched by the short-term period of instability in the full-order response, showing that the linearized system with neglected thermal effects does reflect the stability characteristics of the full ATE system. The same observation can be made in zone II, although the dynamic “instability” is very benign in this case. An apparently spurious prediction of instability is also present at roughly five seconds; this corresponds to a high-frequency mode which does not participate in the response before regaining stability. The disparate levels of response between different unstable regions of the trajectory reinforce the argument for consideration of nonlinear postflutter dynamics.

An area of concern is zone III, where linearization yields no evidence of instability. Because the zone III instability is related to low panel stiffness rather than a classical unstable damping ratio, the linearized detection criteria fail. Indeed, the instability is amplitude-dependent and cannot be exhibited by a linear system. Put another way, the equilibrium is asymptotically stable but possesses only a finite domain of attraction. This can be demonstrated via simulation.

The final converged quasi-static increment was used as a restart point for an Abaqus/UDF, L-3P, and L-LP model. No NLROM was available at this temperature level, so no NL-3P model was used. A slight uniform pressure (100 Pa) was applied to each model for a period of 1 ms to induce an initial response. A second L-3P run was conducted with only a 50 Pa initial pressure applied, resulting in an initial condition reduced by 50%. The results are plotted in Figure 9.

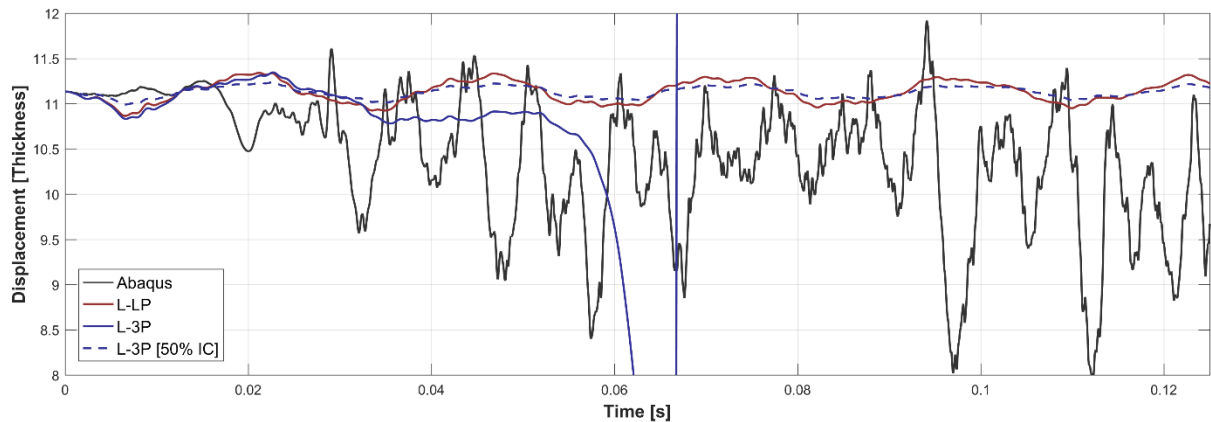


**Figure 9: Demonstration of amplitude-dependent instability at high temperatures/deflections of the ATE model. An Abaqus/UDF, L-LP, and two L-3P responses are shown; the L-3P response with initial conditions cut by 50% remains stable while the L-3P model with full-strength initial conditions diverges.**

The Abaqus solution oscillates at low frequency for just over a full period before entering a high-amplitude LCO, as observed in Figure 8. The L-LP model enters a similar low-frequency oscillation but remains stable over the entirety of the response history. Similar behavior is observable in the L-3P solution initiated with 50% strength initial conditions. Critically, though, the same L-3P model is pulled into a severe instability when the initial conditions are increased to full strength and it leaves the stable domain of attraction of the equilibrium.

Such instabilities are not straightforward to treat in an a posteriori manner. If insufficiently large initial conditions are selected, a particular integration will never leave the stable domain of attraction. Even if sufficient energy is imparted into a structure, an initial configuration may be chosen such that the unstable domain is missed. The only reliable way to determine the boundaries of the domain of attraction is through a suitable a priori method using an analytical model. Application of Lyapunov's second method to this task is a likely candidate for future investigation.

## VI. Summary and Further Work

This work has demonstrated the utility and reinforced the necessity of using nonlinear structural models in conjunction with nonlinear aerodynamics to obtain accurate postflutter behavior of thin panel aerostructures. Including nonlinear aerodynamics when only a linear structural model is available does not provide accurate LCO amplitudes for the structure. On the other hand, if an analyst or designer is interested only in classical asymptotic flutter boundaries, neither nonlinear structural nor aerodynamic effects need be considered, as the linearized system is entirely sufficient for computation of asymptotic stability.

Tempering this statement are results from an ATE case study, which showed that the linearized model could accurately predict moderate-amplitude LCOs during the structure's thermal transient but missed entirely a highly unstable region caused by high temperatures and large deflections. In this case, linearized analysis failed due to the presence of an amplitude-dependent instability. The existence of such instabilities in this type of system is troubling, as they are potentially difficult to locate using common a posteriori stability evaluation methods for nonlinear dynamic systems. For the case studied in this paper, nonlinear aerodynamics led to the amplitude-dependent instability. In general, however, structural effects such as buckling or snap-through may also cause the structure to depart from a nominally stable equilibrium point.

Several potential areas for future work have been identified. A noticeable discrepancy exists between the flutter boundary predicted using piston theory approaches and the boundary estimated from CFD analysis. To bring the piston theory results into line with those predicted by CFD, a procedure to obtain a CFD-corrected piston theory was convincingly demonstrated in reference [1]. A nonlinear form of corrected piston theory was used in that work; it should be possible to extend the linearization procedure demonstrated in this paper to the CFD correction procedure, obviating the need for numerical integration of the resulting system.

Moving beyond the fully linear setting, it should be possible to use Lyapunov's second method to obtain a configuration space corresponding to the stable region of attraction of the nonlinear system. In conjunction with asymptotic stability predictions from a fully linearized model, this capability would provide a priori flutter boundaries and knowledge of any amplitude-dependent instabilities across a quasi-static ATE time history without the need for nonlinear structural modeling.

If postflutter response amplitudes are of interest, NLROMs are a necessity for efficient response evaluation. Constructing NLROMs of single structures is a fairly well-understood process (in contrast to nonlinear substructuring, which remains an area of active research). However, no commercially available capability exists to generate NLROMs; the existing codes are academic/research-oriented in nature. Additionally, the generation of NLROMs for thermally deflected structures is difficult and not well understood, although the alternative approach of generating a thermally coupled NLROM that can deflect accurately in response to thermal loads does show promise [33]. Using a thermoelastic NLROM in conjunction with piston theory and Eckert's reference enthalpy for fully coupled, dynamic ATE response prediction is an application of significant interest.

Finally, even if a structural NLROM is generated and accurate nonlinear aerodynamic loads are provided, the model is of little use if its characteristics cannot be properly and conveniently identified. Various a priori methods exist for the analysis of nonlinear systems. The harmonic balance method, for instance, is a likely candidate. The system examined in this work was used in an exploratory study of numerical continuation methods, with promising results [45]. Work on this area will continue, with the objective of moving from numerical to analytical continuation procedures without loss of predictive accuracy.

Taken together, application of the methods discussed in this paper and postulated above will provide analysts and designers with the ability to make informed choices regarding structure and trajectory for future hypersonic vehicles.

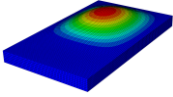
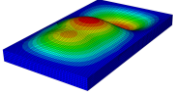
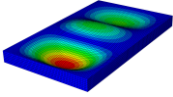
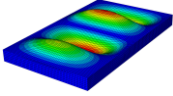
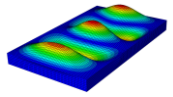
## Appendix: Reduced-Order Model Construction

This appendix gives a very brief overview of the construction and validation process used to generate the linear and nonlinear reduced-order models.

Modes of the structure were computed at the dry spring equilibrium and the flow equilibrium positions. This latter set of modes includes geometrically nonlinear effects induced by the external pressure field but does not include any aerodynamic stiffness terms. Since these modes do not contain stiffness contributions from the fluid loading, they are referred to as “flow-loaded” modes rather than “wet” modes. Frequencies and mode shapes for selected modes are shown in Table 2.

The number of structural modes required to obtain an accurate flutter boundary solution was assessed by sequentially computing the flutter boundary using a sequentially increasing number of modes, as depicted in Figure 10. The process was then repeated, including modes according to the order in which they participated in the time integration of Figure 3, based on the RMS value of each modal coordinate. The resulting curve is also shown in Figure 10. Based on these results, five modes were selected for inclusion in the NLROM: modes 1, 2, 3, 5, and 8, as shown in Table 2.

**Table 2: Summary of first five aeroelastically important modes. Frequency shifts between dry and flow-loaded modes are reported; the mode shapes in each set are visually indistinguishable from each other.**

Mode	Frequencies [Hz]		Plot
	Dry	Flow-Loaded	
1	96.5	101.4	
2	166.6	169.1	
3	183.7	184.9	
5	281.61	284.7	
8	390.74	392.5	

Some difficulty was encountered in generating an NLROM using the modes at bias spring equilibrium. This may be a result of the spring inducing a fairly benign snap-through behavior in the panel, which is traditionally difficult to model. As such, instead of using the spring equilibrium modes, flat-panel modes were selected as the basis set for the NLROM. These were obtained by eliminating the initial deflection in the bias spring, although the spring stiffness itself was retained in the FEM. Generation of the nonlinear restoring force of Equation (14) required 130 static load cases with five modes included in the nonlinear basis.

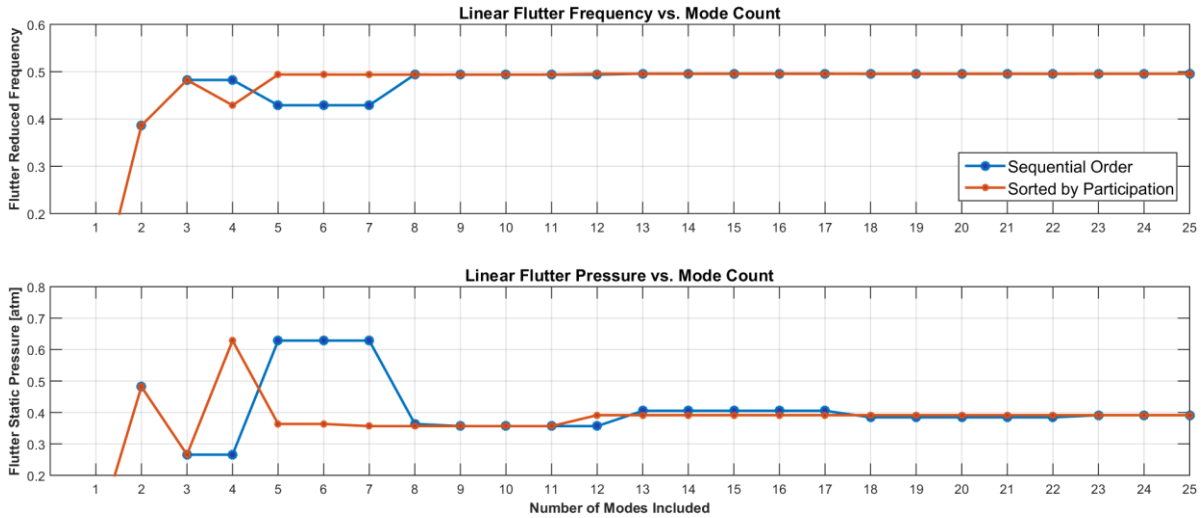


**Figure 10: Convergence of flutter frequency (top) and flutter pressure (bottom) for the L-LP model at reference Mach and temperature. “Sequential order” indicates that modes were added in order of ascending natural frequency, whereas “Sorted by Participation” indicates that modes were added according to their participation in an L-3P nonlinear time integration, sorted by RMS modal amplitude.**

To assess the sufficiency of the mode set selected for the NLROM, a pair of nonlinear normal mode (NNM) backbone curves were computed corresponding to a two-mode and five-mode nonlinear model. The NNM backbone is a set of periodic responses of the nonlinear system, computed at various energy levels [46]. NNMs are a useful method for assessing the convergence of NLROMs, as they provide a load-independent metric for the dynamic nonlinear behavior of the system [47]. Figure 11 depicts the frequency-energy evolution of the NNMs initiating at mode 2, with the deformation plots depicting the change in mode shape as a function of increasing energy. Since the two curves match each other quite well, the nonlinear dynamics of the panel are considered sufficient when modeled using five modes.

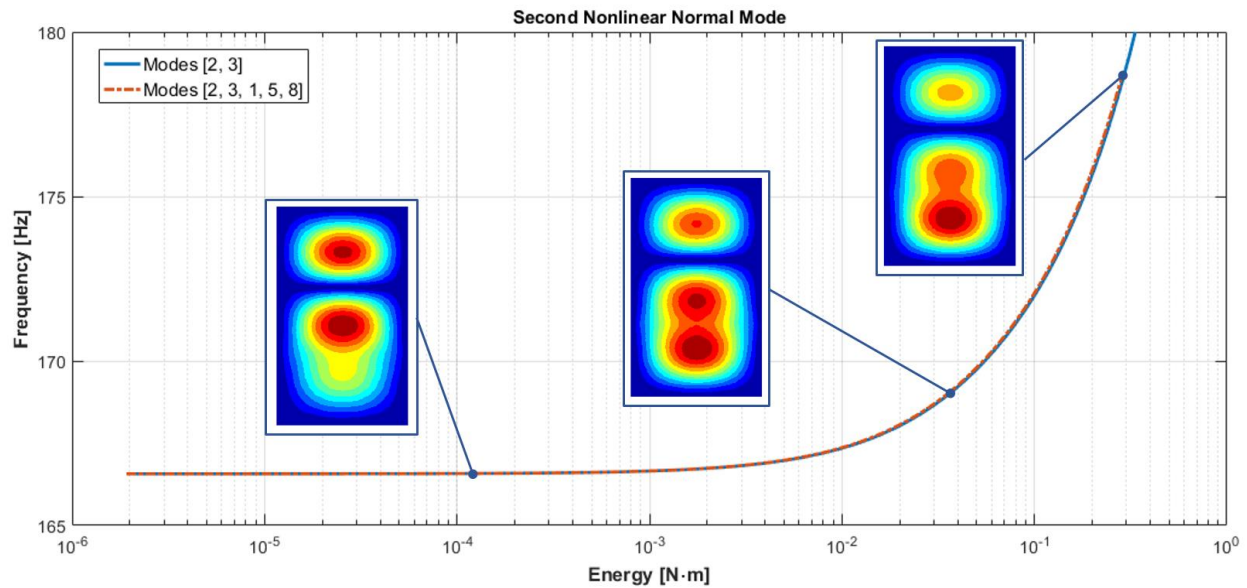


**Figure 11: Nonlinear normal mode backbone curve for mode 2 of the panel, demonstrating convergence of the NLROM between a two-mode and five-mode model.**

## Acknowledgments

This material is based upon work supported by the United States Air Force under Contract No. FA8650-15-C-2573. The authors also gratefully acknowledge the support of Dr. S. Michael Spottswood, technical monitor. The contributions of ATA employees Scott Miskovish, Michael Nucci, and Eric Blades in developing both the general co-simulation framework and the approximate hypersonic simulation system were also essential for the completion of this study.

## References

- [1] J. McNamara, R. Crowell, P. Friedmann, B. Glaz and A. Gogulapati, "Approximate Modeling of Unsteady Aerodynamics for Hypersonic Aeroelasticity," *Journal of Aircraft*, pp. 1932-1945, 2010.
- [2] R. Eckert and G. Ernst, "Survey on Heat Transfer at High Speeds," Armed Services Technical Information Agency, Arlington, VA, 1962.
- [3] A. J. Culler and J. J. McNamara, "Impact of Fluid-Thermal-Structural Coupling on Response Prediction of Hypersonic Skin Panel," *AIAA Journal*, vol. 49, no. 11, pp. 2393-2406, 2011.
- [4] L. Librescu, P. Marzocca and W. A. Silva, "Supersonic/Hypersonic Flutter and Postflutter of Geometrically Imperfect Circular Cylindrical Panel," *Journal of Spacecraft and Rockets*, vol. 39, no. 5, pp. 802-812, 2002.
- [5] I. Nydick, P. P. Friedmann and X. Zhong, "Hypersonic Panel Flutter Studies on Curved Panels," in *36th Structures, Structural Dynamics and Materials Conference*, New Orleans, 1995.
- [6] F. Sabri and A. A. Lakis, "Finite Element Method Applied to Supersonic Flutter of Circular Cylindrical Shells," *AIAA Journal*, vol. 48, no. 1, pp. 73-81, 2010.
- [7] R. J. Klock and C. E. S. Cesnik, "Aeroelastic Stability of High-Speed Cylindrical Vehicles," in *AIAA SciTech Forum*, Grapevine, TX, 2017.
- [8] E. Carrera and E. Zappino, "Aeroelastic Analysis of Pinched Panels in Supersonic Flow Changing with Altitude," *Journal of Spacecraft and Rockets*, vol. 51, no. 1, pp. 187-199, 2013.
- [9] M. D. Olson and Y. C. Fung, "Comparing Theory and Experiment for the Supersonic Flutter of Circular Cylindrical Shells," *AIAA Journal*, vol. 5, no. 10, pp. 1849-1855, 1967.
- [10] J. J. Nichols, "Final Report: Saturn V, S-IVB Panel Flutter Qualification Test," NASA, Marshall, AL, 1969.
- [11] M. J. Neufeld, "A Young Man, of Very Germanic Appearance," in *Von Braun: Dreamer of Space, Engineer of War*, Vintage Books, New York, 2007, pp. 181-182.
- [12] G. H. Jordan, N. J. McLeod and L. D. Guy, "Structural Dynamic Experiences of the X-15 Airplane," NASA, Washington, D.C., 1962.
- [13] S. C. Dixon, G. E. Griffith and H. L. Bohon, "Experimental Investigation at Mach Number 3.0 of the Effects of Thermal Stress and Buckling on the Flutter of Four-Bay Aluminum Alloy Panels with Length-Width Ratios of 10," NASA, Washington, D.C., 1961.
- [14] M. P. Mignolet, A. Przekop, S. A. Rizzi and S. M. Spottswood, "A Review of Indirect/Non-Intrusive Reduced Order Modeling of Nonlinear Geometric Structures," *Journal of Sound and Vibration*, vol. 332, pp. 2437-2460, 2013.
- [15] S. A. Rizzi and A. A. Muravyov, "Determination of Nonlinear Stiffness with Application to Random Vibration of Geometrically Nonlinear Structures," *Computers and Structures*, vol. 81, no. 15, pp. 1513-1523, 2003.
- [16] J. J. Hollkamp, R. W. Gordon and S. M. Spottswood, "Nonlinear Modal Models for Sonic Fatigue Response Prediction: A Comparison of Methods," *Journal of Sound and Vibration*, vol. 284, no. 3, pp. 1145-1163, 2005.
- [17] E. Luke, "On Robust and Accurate Arbitrary Polytope CFD Solvers (Invited)," in *AIAA Computational Fluid Dynamics Conference*, Miami, 2007.

- [18] E. Blades, S. Miskovich, E. Luke, E. Collins and A. Kurkchubashe, "Multiphysics Simulation Capability using the SIMULIA Co-Simulation Engine," in *20th AIAA Computational Fluid Dynamics Conference*, Honolulu, 2011.
- [19] E. Blades, P. Shah, M. Nucci and S. Miskovich, "Demonstration of Multiphysics Analysis Tools on Representative Hypersonic Vehicle Structures," in *54th AIAA Structures, Structural Dynamics, and Materials Conference*, Boston, 2013.
- [20] E. L. Blades, N. D. Reveles, M. Nucci and M. Maclean, "Fully Coupled Aero-Thermochemical-Elastic Simulations of an Eroding Graphite Nozzle," in *Proceedings from the 64th JANNAF Propulsion Meeting/31st Rocket Nozzle Technology Meeting*, Kansas City, 2017.
- [21] S. Flores, A. Gokce, J. Buck, J. Davis, M. Porter, B. Sutton and S. Violette, *Predicting Nonlinear Response of Carbon-Based Composite Materials*, Indian Wells, CA: National Space & Missile Materials Symposium, 2017.
- [22] W. T. Strike, "Calibration and Performance of the AEDC/VKF Tunnel C, Mach Number Aerothermal Wind Tunnel," AEDC TR-82-6, 1982.
- [23] P. N. Shah, E. L. Blades, M. Nucci, J. Schoneman, D. Berg, A. Cornish and T. Hill, "Nonlinear Dynamic Response of Hypersonic Vehicle Skin Panels Using Coupled Fluid-Thermal-Structural Simulation Tools," in *International Modal Analysis Conference*, Anaheim, 2017.
- [24] E. H. Dowell, "Panel Flutter: A Review of the Aeroelastic Stability of Plates and Shells," *AIAA Journal*, vol. 8, no. 3, pp. 385-399, 1970.
- [25] C. Mei, K. Abdel-Motagaly and R. Chen, "Review of Nonlinear Panel Flutter at Supersonic and Hypersonic Speeds," in *Langley International Forum on Aeroelasticity and Structural Dynamics*, Hampton, VA, 1999.
- [26] J. J. M. Friedmann and P. P., "Aeroelastic and Aerothermoelastic Analysis in Hypersonic Flow: Past, Present, and Future," *AIAA Journal*, vol. 49, no. 6, pp. 1089-1122, 2011.
- [27] R. C. Zhou, D. Y. Xue and C. Mei, "On Analysis of Nonlinear Panel Flutter at Supersonic Speeds," in *First Industry/Academy Symposium on Research for Future Supersonic and Hypersonic Vehicles*, Greensboro, NC, 1994.
- [28] K. Kim, Y. Kim, M. Mignolet, D. Liu, P. Chen and D. Lee, "Random Aeroelastic Response Due to Strong Hypersonic Unsteady-Wave/Shock Interaction with Acoustic Loads," in *Proceedings of the 48th Structures, Structural Dynamics, and Materials Conference*, Honolulu, 2007.
- [29] D. Liu, P. Chen, Z. Zhang, Z. Wang, S. Yang, D. Lee, M. Mignolet, K. Kim, F. Liu, N. Lindsley and P. and Beran, "Continuous Dynamic Simulation of Nonlinear Aerodynamic/Nonlinear Structure Interaction (NANSI) for Morphing Wing Aeroelasticity," in *Proceedings of the 50th Structures, Structural Dynamics, and Materials Conference*, Palm Springs, 2009.
- [30] D. Liu, Z. Wang, S. Yang, C. Cai, X. Wang and M. and Mignolet, "Nonlinear Aeroelastic Methodology for A Membrane-on-Ballute Model with Hypersonic Bow Shock," in *Proceedings of the 50th Structures, Structural Dynamics, and Materials Conference*, Palm Springs, 2009.
- [31] R. Perez, X. W. Wang and M. P. Mignolet, "Steady and Unsteady Nonlinear Thermoelastodynamic Response of Panels by Reduced Order Models," in *Proceedings of the 51st Structures, Structural Dynamics, and Materials Conference*, Orlando, 2010.
- [32] A. Matney, R. Perez and M. P. Mignolet, "Nonlinear Unsteady Thermoelastodynamic Response of a Panel Subjected to an Oscillating Flux by Reduced Order Models," in *AIAA Structures, Structural Dynamics, and Materials Conference*, Denver, 2011.
- [33] A. Gogulapati, K. Brouwer, X. Q. Wang, R. Murthy, J. J. McNamara and M. Mignolte, "Full and Reduced Order Aerothermoelastic Modeling of Built-Up Aerospace Panels in High-Speed Flows," in *AIAA Structures, Structural Dynamics, and Materials Conference*, Grapevine, TX, 2017.
- [34] L. Meirovitch, *Methods of Analytical Dynamics*, New York: McGraw-Hill, 1970.



- [35] P. Parks, "A Stability Criterion for Panel Flutter via the Second Method of Liapunov," *AIAA Journal*, vol. 4, no. 1, pp. 175-177, 1966.
- [36] C. Kuo, L. Morino and J. Diugundji, "Perturbation and Harmonic Balance Methods for Nonlinear Panel Flutter," *AIAA Journal*, vol. 10, no. 11, pp. 1479-1484, 1972.
- [37] J. N. Juang and R. S. Pappa, "An Eigensystem Realization Algorithm for Modal Parameter Identification and Model Reduction," *Journal of Guidance, Control, and Dynamics*, vol. 8, no. 5, 1985.
- [38] E. L. Blades, R. S. Miskovish, E. A. Luke, E. M. Collins and A. G. Kurkchubashe, "A Multiphysics Simulation Capability using the SIMULIA Co-Simulation Engine," in *AIAA Computational Fluid Dynamics Conference*, Honolulu, Hawaii, 2011.
- [39] M. J. Lighthill, "Oscillating Airfoils at High Mach Number," *Journal of the Aeronautical Sciences*, vol. 20, no. 6, pp. 402-406, 1952.
- [40] W. Rodden, E. Farkas, H. A. Malcom and A. Kliszewski, "Aerodynamic Influence Coefficients from Supersonic Strip Theory: Analytical Development and Computational Procedure," Aerospace Corporation, El Segundo, CA, 1962.
- [41] Siemens PLM Software, "Aeroelastic Analysis User's Guide," Plano, TX, 2014.
- [42] J. Schoneman, "Modal Analysis of Hypersonic Aerostructural Systems," in *International Modal Analysis Conference*, Orlando, 2018.
- [43] M. J. Patil, "Decoupled Second-Order Equations and Modal Analysis of a General Nonconservative System," in *AIAA Dynamics Specialist Conference*, Atlanta, 2000.
- [44] R. W. Gordon and J. J. Hollkamp, "Reduced-Order Models for Acoustic Response Prediction," Air Force Research Laboratory, Dayton, 2011.
- [45] J. Schoneman and T. Hill, "Continuation Analysis of Post-Flutter Response in Hypersonic Flow," in *International Modal Analysis Conference*, Orlando, 2018.
- [46] G. Kerschen, M. Peeters, J. C. Golinval and A. F. Vakakais, "Nonlinear normal modes, Part I: A useful framework for the structural dynamicist," *Mechanical Systems and Signal Processing*, vol. 23, no. 1, pp. 170-194, 2009.
- [47] R. J. Kuether, M. R. Brake and M. S. Allen, "Evaluating Convergence of Reduced Order Models Using Nonlinear Normal Modes," *Model Validation and Uncertainty Quantification*, vol. 3, pp. 287-300, 2014.